Organic LETTERS

Letter

pubs.acs.org/OrgLett

Stabilization of a Strained Heteroradialene by Peripheral Electron Delocalization

S. Hessam M. Mehr, Brian O. Patrick, and Mark J. MacLachlan*

Department of Chemistry, University of British Columbia, 2036 Main Mall, Vancouver, BC V6T 1Z1, Canada

Supporting Information

ABSTRACT: Dimethylamine and 2,4,6-triformylphloroglucinol react to form a product with a highly contorted nonplanar geometry due to favorable electron delocalization. This new heteroradialene compound has been studied by X-ray diffraction, variable-temperature multinuclear NMR spectroscopy, IR spectroscopy, UV−vis spectroscopy, and ab initio calculations. Electron delocalization throughout the periphery of the central ring leads to a structure that retains very little of the aromatic characteristics of the starting material.

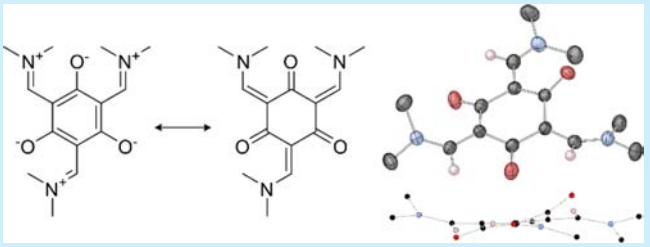

Electron delocalization within conjugated molecules is a versatile chemical concept that is at the root of fundamental phenomena including the aromaticity of benzene, the acidity of carboxylic acids, and the properties of biologically relevant molecules such as vitamin A (retinal),[1] vitamin B6 (pyridoxal phosphate),[2] and chlorophyll.[3] Controlled delocalization of electrons is central to the design of modern electronic devices[4] and, in the case of π electrons, has given rise to the exciting properties of graphene and its derivatives.[5,6]

In 2003, we reported a new family of heteroradialenes that are prepared from the Schiff base condensation of 2,4,6-triformylphloroglucinol **1** and primary amines (Scheme 1a).[7] Surprisingly,

Scheme 1. Reactions of 1 with a Primary Amine (a) and Dimethylamine (b)

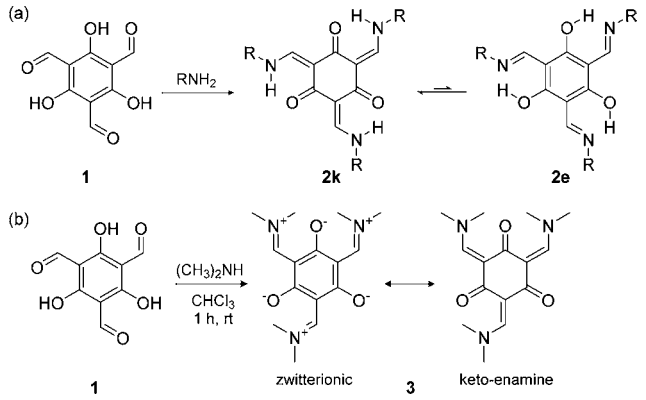

these new tris(salicylaldimine) molecules **2** (TSANs) exist exclusively as the keto-enamine tautomer **2k** rather than the expected enol-imine tautomer **2e**. While the keto-enamine motif has been exploited in a variety of discrete and extended structures,[7−16] little work has been done to explain its dominance over the canonical enol-imine structure. These new molecules challenge our notions of aromaticity and beg the following questions: What stabilizes the TSANs to compensate for the loss of aromaticity in **2k** vs **2e**? Does the additional stabilization arise exclusively from improved hydrogen-bonding interactions, or is there another explanation?

To investigate these questions, we prepared compound **3** by reacting **1** with a secondary amine. Using a secondary amine allows us to evaluate the propensity of the electronic structure to favor the keto-enamine form in the absence of changes in the σ skeleton or the influence of hydrogen bonding.[17] We expected **3** to have an aromatic zwitterionic structure, but our experiments show that the push−pull interaction of the charged side chains undermines aromaticity and introduces a new mode of electron delocalization. Here, we describe our detailed structural, spectroscopic, and computational studies of compound **3**. These findings illustrate the promise of alternative electron delocalization motifs and contribute to a better structural understanding of TSANs.

Compound **3** was prepared in 99% yield by bubbling an excess of gaseous dimethylamine into a suspension of **1** in chloroform (Scheme 1b). The reaction is complete in 1 h at room temperature (rt), and evaporation of solvent gives the product as a bright yellow-orange solid that is stable in the absence of oxygen and water. Compared to TSANs **2k**/**2e**, **3** replaces the labile NH/OH hydrogen atoms with methyl groups, preventing intramolecular hydrogen bonding or tautomerization—the zwitterionic and keto-enamine forms of **3** are resonance structures rather than tautomers.

Slow evaporation of a solution of **3** in a mixture of hexanes and dichloromethane yielded orange crystals suitable for single-crystal X-ray diffraction (SCXRD). The solid-state molecular structure of **3** reveals a highly distorted, asymmetric structure (Figure 1a). Compared to the planar core observed for TSANs

Received: February 29, 2016
Published: March 31, 2016

DOI: 10.1021/acs.orglett.6b00577
Org. Lett. 2016, 18, 1840−1843

prepared from reacting **1** with a primary amine (i.e., **2k**, Figure 1b), oxygen atoms O^1 and O^2 in **3** have surprisingly large deviations from the mean plane of the molecule (31 and 18°, respectively).

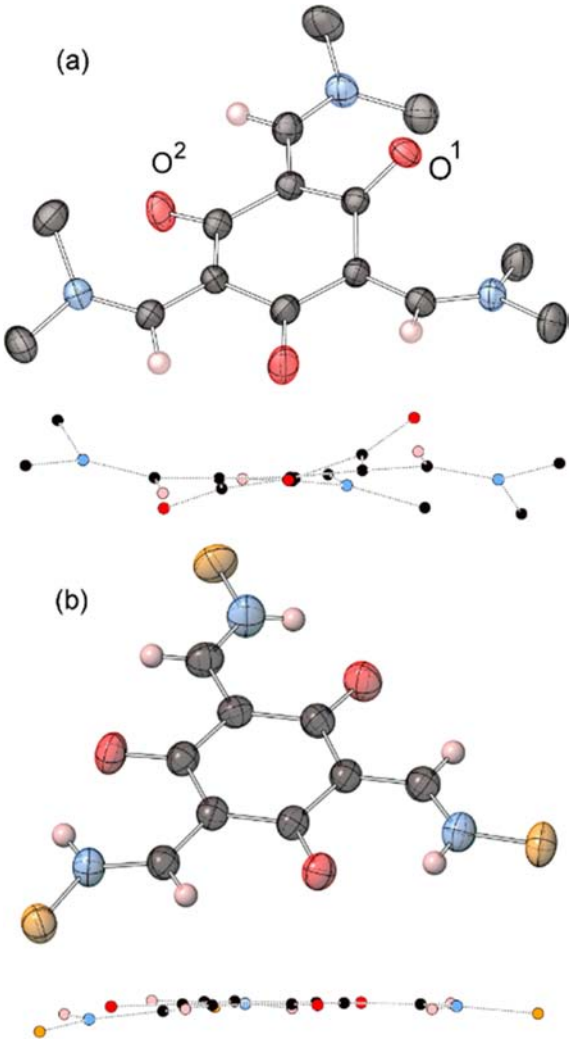

Figure 1. (a) Solid-state molecular structure of **3** with methyl hydrogen atoms omitted for clarity. (b) Representative keto-enamine tautomer **2k**, with yellow atoms showing truncated ($CH(CH_2OH)CH_2CH_3$) groups.[18]

The large displacements of O^1 and O^2 can be understood by examining their proximity to the methyl groups, where two methyl groups push O^1 out of the plane and one pushes O^2 out of the plane (Figure 2). Partial coplanarity of the side chains with the central ring allows electron delocalization between the formal phenoxide and iminium units, hence the close oxygen−methyl contacts. Ab initio geometry optimization of this structure in isolation relaxes the strain negligibly, suggesting that the observed molecular shape is not merely due to interactions in the crystalline phase. Another notable feature is that the compound crystallized reproducibly as the asymmetric form rather than the C_{3h} symmetric form generally observed in the crystal structures of keto-enamines **2k**.

Bond lengths in **3** (Table 1) resemble those of keto-enamine rather than enol-imine TSANs. In fact, the departure from aromaticity and toward the keto-enamine structure in **3** is stronger than that of typical keto-enamines **2k**. Corresponding

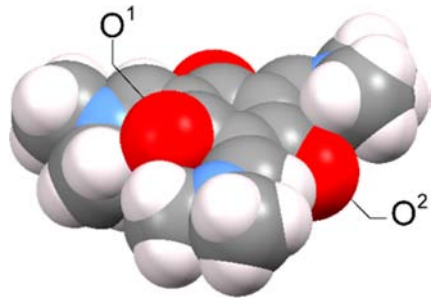

Figure 2. Space-filling diagram derived from the SCXRD structure of **3**.

Table 1. Bond Lengths of Compound 3 and Comparable Molecules

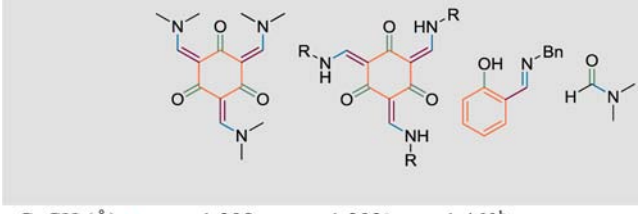

C–CH (Å) ●	1.398	1.392[a]	1.460[b]	–
CH–N ●	1.320	1.293	1.276	1.341
C–O ●	1.253	1.261	1.357	1.231
C–C ●	1.462	1.446	1.386	–

[a]Representative keto-enamine shown in Figure 1b (R = CH-(CH_2OH)CH_2CH_3).[18] [b]Representative enol-imine from the literature.[19]

bond lengths of *N*,*N*-dimethylformamide are very close, as well. Thus, **3** might be described as an amide in which the electronic coupling between the C═O and NRR′ groups is mediated by the central ring, with this mode of delocalization replacing classic aromaticity.

Given the unusual solid-state structure of **3**, we undertook a study of its solution dynamics using variable-temperature (VT) NMR spectroscopy. At rt, the ^{1}H NMR spectrum of **3** in toluene-d_8 shows broad CH_3 signals around 3 ppm, with only one broad resonance at 8.15 ppm for the CC*H*N groups. This is consistent with rapid rotation about the C−CH bonds, which we next attempted to impede at low temperature. Thus, at −89 °C, eight peaks are seen near 3 ppm and four near 8 ppm, due to the discrete symmetric (**3s**) and asymmetric (**3a**) forms of **3** (Figure 3). The symmetric form contributes two distinct peaks for CH_3 groups and one CH resonance; the asymmetric form produces six distinct peaks for CH_3 groups and three distinct CH resonances. Heating the sample above 60 °C causes coalescence of the peaks assigned to the methyl protons, indicating facile rotation about both the CH−N and C−CH bonds.

The same general behavior is observed in other solvents. Table 2 shows the coalescence temperatures (T_c) and free energies of activation for rotation ($\Delta G^{\ddagger}_{rot}$) about the C−CH and CH−N bonds calculated using the Eyring model. These $\Delta G^{\ddagger}_{rot}$ values are in good agreement with those previously reported for γ-keto-enamines.[20] The remarkably low $\Delta G^{\ddagger}_{rot}$ (C−CH) and high $\Delta G^{\ddagger}_{rot}$ (CH−N) in CD_3OD could be indicative of larger zwitterionic characteristics in CD_3OD, likely due to better stabilization of the negative charge on the oxygen atoms through hydrogen bonding.

At low temperature, the relative areas of the peaks on the ^{1}H NMR spectrum of **3** can be used to calculate the **3s**/**3a** ratio. This

DOI: 10.1021/acs.orglett.6b00577
Org. Lett. 2016, 18, 1840−1843

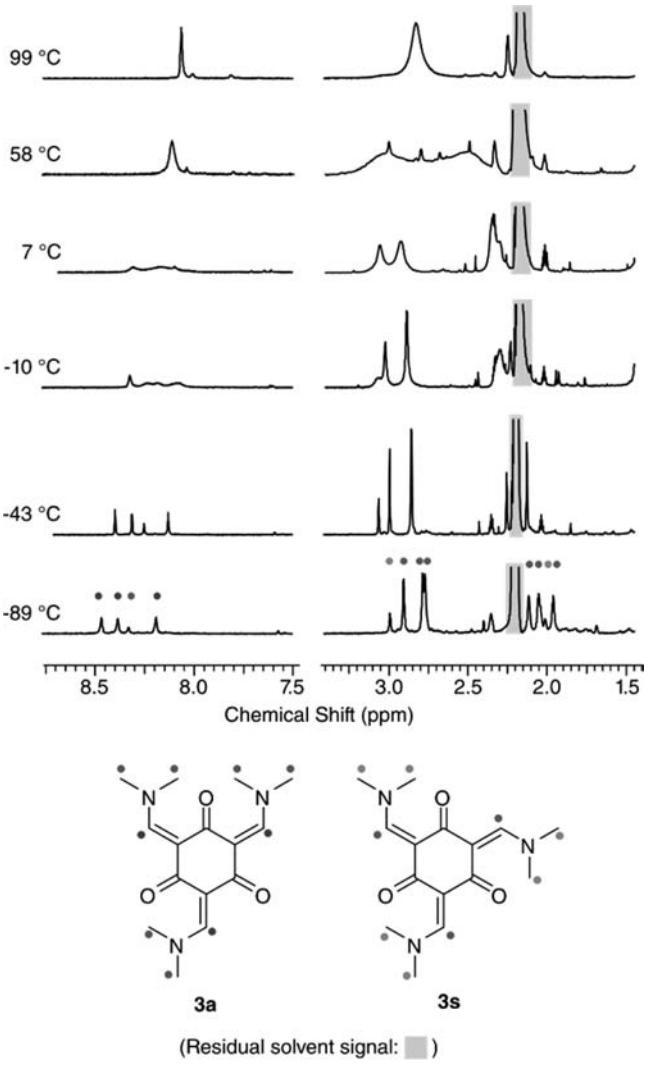

Figure 3. VT ^{1}H NMR spectrum of **3** in toluene-d_8 and the two distinct structures seen at −89 °C.

Table 2. Coalescence Temperatures (T_c) and Activation Energies for Bond Rotation ($\Delta G^{\ddagger}_{rot}$) for 3 from VT NMR

	C−CH rotation			CH−N rotation		
	T_c (°C)	$\Delta\nu$ (Hz)	$\Delta G^{\ddagger}_{rot}$ (kJ/mol)[a]	T_c (°C)	$\Delta\nu$ (Hz)	$\Delta G^{\ddagger}_{rot}$ (kJ/mol)[a]
toluene-d_8	7	122	57	60	250	64
DMF-d_7	−3	75	54	45	188	62
methanol-d_4	<−89	47	<37	>58	138	>65

[a] $\Delta G^{\ddagger}$ values are ±2 kJ/mol.

ratio is solvent-dependent and can be as large as 1:5 in toluene-d_8. Ab initio calculations show that the geometry obtained in the solid state (Figure 1a), when energy-optimized, is slightly more stable than other possible asymmetric isomers. We therefore suspect that the dominant form of **3** in solution at low temperature (**3a**) corresponds to that observed in SCXRD.

A number of studies have demonstrated the utility of ^{15}N NMR as a sensitive probe in the study of tautomeric species. Changes in the tautomeric state have been shown to alter the ^{15}N chemical shift by more than 100 ppm.[21−23] Simple enamines have chemical shifts in the 50−80 ppm range,[24] whereas imines have chemical shifts above 200 ppm. We therefore undertook a ^{15}N NMR study of isotopically labeled **3** to gauge the relative contributions of keto-enamine and zwitterionic characteristics.

The ^{15}N-labeled analogue of **3**, **3**-$^{15}\mathbf{N}_3$, was synthesized by reacting **1** with excess $^{15}NH(CH_3)_2$. In CD_3OD (at rt), the ^{15}N NMR spectrum of this compound gives a single sharp resonance at 130.2 ppm, between the reported enamine and imine chemical shift ranges. Next, the temperature dependence of the ^{15}N signal was examined via indirect measurement using ^{1}H−^{15}N HSQC (J_{NH} = 12 Hz). In CD_2Cl_2, a very broad ^{15}N signal results at rt that resolves to three distinct resonances upon cooling below −20 °C. As Figure 4 shows, each ^{15}N peak is coupled to two methyl ^{1}H

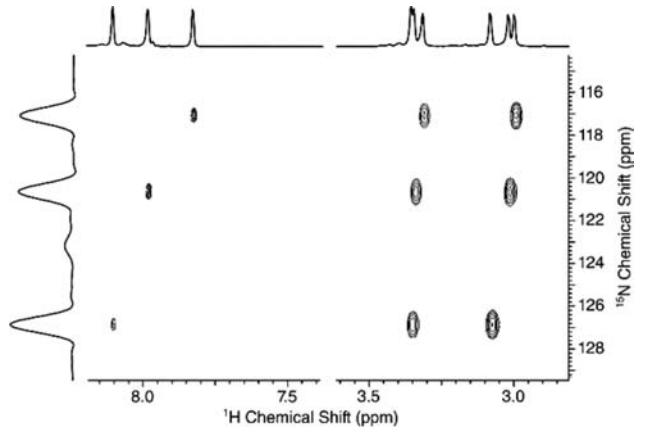

Figure 4. ^{1}H−^{15}N HSQC spectrum of **3**-$^{15}\mathbf{N}_3$ at −84 °C (CD_2Cl_2, 400 MHz).

signals. An additional weak ^{15}N resonance (seen on the ^{15}N projection) appears to be due to the symmetric form. The measured ^{15}N chemical shifts are in the 115−130 ppm range throughout the temperature range studied. These values are in good agreement with those reported for cyclic γ-keto-enamines (110−150 ppm)[24] and suggest that the electron distribution in **3** is keto-enamine-like regardless of temperature.

In general, ^{15}N chemical shift values moved downfield by ∼15 ppm when methanol-d_4 was used as solvent. Other researchers have reported that ^{15}N signals move upfield in polar solvents or when hydrogen bonding is present.[25] We suspect that this exceptional behavior can be attributed to the amplified zwitterionic characteristics of **3** in methanol, consistent with our VT ^{1}H NMR experiments.

Comparing the infrared spectra of **3** and **3**-$^{15}\mathbf{N}_3$ gives further information about bonding in **3**. The intense absorption at 1582 cm^{-1} in **3** experiences a small red shift of ∼9 cm^{-1} (0.6%) to 1573 cm^{-1} in **3**-$^{15}\mathbf{N}_3$, and values closer to the expected C^{14}N/C^{15}N isotope shift of 1.5% are only seen for the weak resonances around 1200 cm^{-1}. Ab initio analysis of the vibrational modes in **3** indicates that the normal modes around 1600 cm^{-1} correspond to strongly coupled C−O/CH−N stretches. In this light, the intermediate isotope shift obtained is not surprising given the mixed nature of these vibrational modes. On the other hand, the peaks around 1200 cm^{-1} arise due to relatively pure N−CH_3 stretches and undergo the expected isotope shift.

In the presence of air, compound **3** is transformed into an intractable sticky red mass over a period of days at rt. The yellow-orange color of **3** in crystalline and solution form, however, seems to originate from **3** and not any contaminants. In fact, time-dependent density functional theory calculation of the electronic excited states of **3** closely matched the UV−vis absorption peaks at 363 and 308 nm (calcd 350 and 325 nm).

DOI: 10.1021/acs.orglett.6b00577
Org. Lett. 2016, 18, 1840−1843

Our calculations show that the former excitation is principally from HOMO (mostly radialene C═CH π) to LUMO (C═O and CH═N π^*) and the latter from HOMO−1 (O lone pairs and ring σ^*) to LUMO.

Given the stability of **3** under an inert atmosphere, we also used cyclic voltammetry to probe its reactivity. In CH_2Cl_2, compound **3** shows two irreversible oxidation events at 0.99 and 1.23 V (referenced to ferrocence at 0.44 V), with no reduction events within the solvent potential window.

Finally, considering the enormous strain in **3** due to the methyl groups, we explored the possibility of adding even more strain by synthesizing analogues of **3** with bulkier substituents on the nitrogen atom. As expected, these analogues are formed substantially less readily. Thus, **1** slowly reacts with a large excess of diethylamine to give compound **4** overnight (Scheme 2), while the same reaction using diisopropylamine only consumes 1−2 equiv of amine even after 72 h at 55 °C, and we could not isolate the fully substituted product.

Scheme 2. Reaction of 1 with Diethylamine

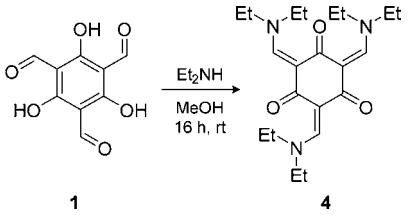

1 **4**

In conclusion, we have shown that charge redistribution throughout the periphery of TSANs is an alternative mode of electron delocalization that has a stabilizing effect outweighing that of aromaticity. Interestingly, peripheral delocalization prevails even when it requires a highly crowded geometry. We expect that powerful driving forces of this type can be exploited to drastically alter the structure and reactivity of other organic molecules.

■ ASSOCIATED CONTENT

Supporting Information

The Supporting Information is available free of charge on the ACS Publications website at DOI: 10.1021/acs.orglett.6b00577.

Improved synthesis of **1**, synthesis and characterization of **3**, **3**-$^{15}N_3$, and **4**, expanded ab initio section, and energy-optimized atomic coordinates for all species used in the calculations (PDF)

Crystal structure of **3** (CIF)

■ AUTHOR INFORMATION

Corresponding Author

*E-mail: mmaclach@chem.ubc.ca.

Notes

The authors declare no competing financial interest.

■ ACKNOWLEDGMENTS

We thank NSERC for funding this research (Discovery Grant). S.H.M.M. thanks Jeff Therrien (UBC Chemistry) for assistance with cyclic voltammetry.

■ REFERENCES

(1) Honig, B.; Greenberg, A. D.; Dinur, U.; Ebrey, T. G. *Biochemistry* **1976**, *15*, 4593.
(2) Eliot, A. C.; Kirsch, J. F. *Annu. Rev. Biochem.* **2004**, *73*, 383.
(3) Norris, J. R.; Uphaus, R. A.; Crespi, H. L.; Katz, J. J. *Proc. Natl. Acad. Sci. U. S. A.* **1971**, *68*, 625.
(4) Ashcroft, N. W.; Mermin, N. D. *Solid State Physics*, 1st ed.; Holt, Rinehart and Winston, 1976.
(5) Novoselov, K. S.; Geim, A. K.; Morozov, S. V.; Jiang, D.; Katsnelson, M. I.; Grigorieva, I. V.; Dubonos, S. V.; Firsov, A. A. *Nature* **2005**, *438*, 197.
(6) Geim, A. K.; Novoselov, K. S. *Nat. Mater.* **2007**, *6*, 183.
(7) Chong, J. H.; Sauer, M.; Patrick, B. O.; MacLachlan, M. J. *Org. Lett.* **2003**, *5*, 3823.
(8) Sauer, M.; Yeung, C.; Chong, J. H.; Patrick, B. O.; MacLachlan, M. J. *J. Org. Chem.* **2006**, *71*, 775.
(9) Pachfule, P.; Kandmabeth, S.; Mallick, A.; Banerjee, R. *Chem. Commun.* **2015**, *51*, 11717.
(10) Freiherr Von Richthofen, C. G.; Stammler, A.; Bögge, H.; Glaser, T. *Eur. J. Inorg. Chem.* **2012**, *2012*, 5934.
(11) Peng, Y.; Hu, Z.; Gao, Y.; Yuan, D.; Kang, Z.; Qian, Y.; Yan, N.; Zhao, D. *ChemSusChem* **2015**, *8*, 3208.
(12) Kieryk, P.; Janczak, J.; Panek, J.; Miklitz, M.; Lisowski, J. *Org. Lett.* **2016**, *18*, 12.
(13) DeBlase, C. R.; Silberstein, K. E.; Truong, T.-T.; Abruña, H. D.; Dichtel, W. R. *J. Am. Chem. Soc.* **2013**, *135*, 16821.
(14) Shinde, D. B.; Aiyappa, H. B.; Bhadra, M.; Biswal, B. P.; Wadge, P.; Kandambeth, S.; Garai, B.; Kundu, T.; Kurungot, S.; Banerjee, R. *J. Mater. Chem. A* **2016**, *4*, 2682.
(15) Vieweger, M.; Jiang, X.; Lim, Y.-K.; Jo, J.; Lee, D.; Dragnea, B. *J. Phys. Chem. A* **2011**, *115*, 13298.
(16) Jiang, X.; Vieweger, M. C.; Bollinger, J. C.; Dragnea, B.; Lee, D. *Org. Lett.* **2007**, *9*, 3579.
(17) Raczyńska, E. D.; Krygowski, T. M.; Zachara, J. E.; Ośmiałowski, B.; Gawinecki, R. *J. Phys. Org. Chem.* **2005**, *18*, 892.
(18) Suresh, P.; Varghese, B.; Varadarajan, T. K.; Viswanathan, B. *Acta Crystallogr., Sect. E: Struct. Rep. Online* **2007**, *63*, o984.
(19) Elerman, Y.; Paulus, H.; Svoboda, I.; Fuess, H. *Zeitschrift für Krist. - Cryst. Mater.* **1992**, *198*, 135.
(20) Azzaro, M.; Geribaldi, S.; Videau, B. *Magn. Reson. Chem.* **1985**, *23*, 28.
(21) Laxer, A.; Major, D. T.; Gottlieb, H. E.; Fischer, B. *J. Org. Chem.* **2001**, *66*, 5463.
(22) Bojarska-Olejnik, E.; Stefaniak, L.; Witanowski, M.; Webb, G. A. *Bull. Chem. Soc. Jpn.* **1986**, *59*, 3263.
(23) Chan-Huot, M.; Sharif, S.; Tolstoy, P. M.; Toney, M. D.; Limbach, H.-H. *Biochemistry* **2010**, *49*, 10818.
(24) Westerman, P. W.; Roberts, J. D. *J. Org. Chem.* **1977**, *42*, 2249.
(25) Duthaler, R. O.; Roberts, J. D. *J. Am. Chem. Soc.* **1978**, *100*, 4969.

DOI: 10.1021/acs.orglett.6b00577
Org. Lett. 2016, 18, 1840−1843